DOI: 10.1021/cg100806w

CRYSTAL GROWTH & DESIGN
Article
2010, Vol. 10
4516–4525

A Racemic Conglomerate Nipped in the Bud: A Molecular View of Enantiomer Cross-Inhibition of Conglomerate Nucleation at a Surface

Abel Robin,[†] Patrizia Iavicoli,[‡] Klaus Wurst,[§] Matthew S. Dyer,[†] Sam Haq,[†] David B. Amabilino,*[,‡] and Rasmita Raval*[,†]

[†]*Surface Science Research Centre, Department of Chemistry, University of Liverpool, L69 3BX Liverpool, U.K.,* [‡]*Institut de Ciencia de Materials de Barcelona (CSIC), Campus Universitari, 08193 Bellaterra, Catalonia, Spain, and* [§]*Institut für Allgemeine Anorganische und Theoretische Chemie, Universität Innsbruck, A-6020, Innrain 52a, Austria*

Received June 16, 2010; Revised Manuscript Received July 30, 2010

ABSTRACT: The inhibition of conglomerate formation in a racemic monolayer is shown to arise from one enantiomer impeding the growth of homochiral nuclei of the opposite enantiomer. Submolecular level resolution scanning tunneling microscopy (STM) data show that nanometer scale homochiral conglomerate nuclei, containing several tens of molecules, are obstructed from developing further by enantiomeric blockers in their surroundings. We have observed this in the racemic and enantiopure samples of a bis-lactate derivative of resorcinol which was prepared because its size and symmetry made it interesting for the study of chirality in chemisorbed monolayer systems. The solid state racemate forms a racemic compound containing hydrogen bonded chains. The enantiomers and the racemate were deposited onto a Cu(110) surface under ultrahigh vacuum conditions and the monolayers formed were studied by STM, low energy electron diffraction (LEED), and reflection absorption infrared spectroscopy (RAIRS). In particular, STM observations of the racemic monolayer reveal that the individual enantiomers form small organized aggregates which are interrupted by defects of the opposite enantiomer which acts as a growth inhibitor. This situation contrasts sharply with the monolayers formed by the enantiopure compounds, which form large homochiral domains. We believe that this unique nanometer scale view of conglomerate crystallization and its growth inhibition, with each enantiomer acting as a mutual inhibitor of its mirror counterpart in a situation where diffusion is not fast, provides important insights for understanding the formation of conglomerates and racemic compounds in bulk crystals.

Introduction

Molecular level understanding of chirality transmission, and in particular the passage and even amplification of chirality into homochiral systems, is of great importance in a number of scientific and technological areas.[1] The spontaneous resolution of enantiomers in a racemate to form a conglomerate, which arises from the condensation of mirror image molecules into separate domains,[2] is a crucial step toward the preparation of homochiral compounds by crystallization.[3] One thing which can either prevent or favor the emergence of chirality is the inhibition of the growth of homochiral domains, be they in fibers, monolayers, or bulk crystals. A key illustration of this effect is the use of tailor-made inhibitors for the growth of chiral crystals.[4] However, despite great efforts the mapping of chiral nucleation and crystallization at the nanometer scale remains rudimentary and a molecular level view of inhibition has not been reported to the best of our knowledge.

It is particularly interesting to consider what happens in a racemic system in which enantiomers could act as mutual inhibitors for the growth of each other's crystals. Such a situation would surely disfavor conglomerate formation and, instead, give rise to the growth of the racemic compound. In fact, this scenario was raised by Pratt-Brock et al.[5] who pointed out that kinetics may well favor the growth of racemic compound crystals over a conglomerate since half the molecules arriving at the boundaries of a nucleus site are, statistically, of the "wrong" enantiomer. However, for a racemic compound a "wrong" enantiomer occupying a site only has to translate across to the "correct" neighboring site to enable racemic crystal growth to continue. In contrast, during the formation of a conglomerate, the "wrong" enantiomer has no nearby "correct sites" available to diffuse to and, thus, can act as a very effective inhibitor. On this basis, they suggested that if the thermodynamic preference between a conglomerate and a racemic compound is not great, such inhibition effects affecting the kinetics of formation may be the underlying reason why bulk crystalline conglomerates are relatively rare.

The only way one could know of such a phenomenon is to be able to observe directly the nucleation and inhibition process. Given that nucleation of molecules, in general, is considered to be a process in which the condensates have dimensions in the nanometer range,[6] this would require techniques that could probe the system at the nanometer level. During our studies on the spontaneous resolution of compounds at interphases,[7] we have chanced on an example of the inhibition of long-range conglomerate formation by mirror enantiomers at the growing surface-confined crystallite. Thus, the conglomerate nuclei are observed to be confined to very small aggregates of only tens of molecules, by enantiomeric blockers in their surroundings. The technique with which we have observed this process with submolecular resolution is scanning tunneling microscopy (STM).

The unique benefits of STM in the study of chirality within organized molecular monolayers at surfaces has been demonstrated in a number of instances, including identification of the absolute chirality of adsorbates,[8] or the observed enantiomorphous structures of physisorbed[9] and chemisorbed[10] enantiomeric

*To whom correspondence should be addressed. E-mail: amabilino@icmab.es (D.B.A.) and Raval@liv.ac.uk (R.R.).

 Published on Web 09/03/2010

Chart 1

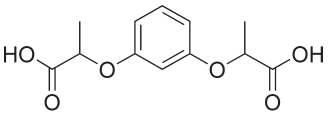

1

and racemic materials. Turning specifically to the creation of conglomerates, we note that the achiral nature of the surfaces in these examples has no enantioselectivity toward chiral molecules. Thus, chirality is introduced by molecular adsorption at the surface and can be understood in terms of a symmetry reduction of the surface upon adsorption: any mirror symmetry of the achiral surface is completely overwritten upon adsorption of enantiomers of chiral molecules, which internally have no mirror symmetry. The enantiomers maintain equal adsorption energy by adopting mirror adsorption geometries leading to local chiral adsorption motifs which spontaneously resolve into mirror enantiomorphs.

The molecule we chose to study the formation of racemates is **1** (see Chart 1), a resorcinol (1,3-dihydroxybenzene) derivative with two chiral lactate acid groups. The choice of the phenyl spacer was to ensure a sufficient size so as to be able to distinguish the enantiomers molecule-by-molecule with the STM on the metal surface. The substitution at the 1,3 positions of the benzene ring was chosen because the molecular assembly has a lower symmetry than the corresponding 1,4 derivatives, a feature which was expected to lead to easier identification of the enantiomers at the molecular level. Specifically, the C_2 axis running through the center of the benzene ring in the 1,4 derivative is not possible in the 1,3 compound. In this way, the symmetry axis normal to the surface is avoided.[11]

Synthesis and Characterization

Compounds (*R*,*R*)-**1** and (*S*,*S*)-**1** were prepared by the synthetic route shown in Scheme 1 for the former (the enantiomer was prepared in an identical way using the enantiomer of methyl lactate as the starting material). In the first step, resorcinol (1,3-dihydroxy benzene) was condensed with (*S*)- or (*R*)-methyl lactate in the presence of triphenylphosphine and diisopropyl azodicarboxylate by means of a Mitsunobu protocol[12] giving, respectively, the ester (*R*,*R*)-**2**, where the stereochemistry is the opposite of the original lactate, in 48% yield after purification by column chromatography. The compounds were characterized by NMR and IR spectroscopies as well as by their optical rotation. The second step was a saponification of these ester derivatives using NaOH in MeOH resulting in (*R*,*R*)-**1** and (*S*,*S*)-**1** as white solids after isolation in 94% yield.

Single crystals of the acids were grown from water. The enantiopure diacid (*R*,*R*)-**1** crystallizes in the orthorhombic $C222_1$ (No. 20) space group with four symmetry-related molecules of (*R*,*R*)-**1** in the unit cell. The structure reveals molecules whose phenoxy group is almost in the same plane as the β-methyl group, with the carboxyl groups located in a pseudo-anti conformation (Figure 1a). This conformation is favored energetically as revealed in theoretical investigations on related compounds.[13] The torsion angle between the carbonyl group and the plane of the phenoxy group ($C_1C_2O_3C_4$ and $C'_1C'_2O'_3C'_4$) is +70.1°. In the crystalline structure, the molecules arrange in homochiral chains which run along the crystallographic *c* axis in which the molecules are linked through hydrogen bonds between the carboxylic groups (see Supporting Information).

Scheme 1. Synthesis of the Chiral Resorcinol Diacid Derivative (*R*,*R*)-1

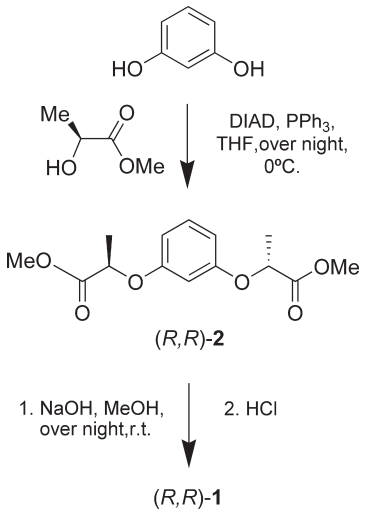

The racemic compound (*R*,*R*)-**1**/(*S*,*S*)-**1** crystallizes in the orthorhombic *Pnna* (No. 52) space group with four molecules in the unit cell. The density of the crystals is higher than those of the enantiopure compound, conforming to Wallach's rule.[5] The crystal structure reveals molecules whose β-methyl group is almost in the same plane as the phenyl ring, with the carboxyl groups located in a pseudoanti conformation (Figure 1b), as is the case for the enantiopure compound. The torsion angle between the carbonyl group and the plane of the phenyl ring for (*R*,*R*)-**1** in the racemic crystal ($C_1C_2O_3C_4$ and $C'_1C'_2O'_3C'_4$) is 72.8°; for (*S*,*S*)-**1** the corresponding angle is −72.8°. Whereas enantiopure (*R*,*R*)-**1** crystallizes forming a hydrogen bonded chain, the (*R*,*R*)-**1**/(*S*,*S*)-**1** crystal contains a hydrogen bonded carboxylic acid dimer across a center of inversion (for all crystallographic information and a details of the packing see Supporting Information).

The solid state IR spectra of the racemic and enantiopure **1** show the single carbonyl adsorption at 1712 cm^{-1} (clearly consistent with strong hydrogen bonding), and the racemic mixture shows overtones and combination bands of ν(CO) and OH deformation vibrations between 2500 and 2700 cm^{-1} and the OH out of plane band at 918 cm^{-1}. The relatively large bandwidth of the 918 cm^{-1} band is characteristic of the centrosymmetric carboxyl dimer. The IR spectra of the enantiopure compound shows two differences from the racemate: first, the carbonyl band is split into two bands at the lower wavenumber and, second, the OH contribution is shifted to a lower frequency (881 cm^{-1}). This difference is a result of the different sheet structures of enantiopure and racemic crystals (as outlined in the Supporting Information, the less rigid OH bond in the catemeric structure of the enantiopure derivative one expects a shift to lower frequencies in the IR).

Monolayers on Cu(110)

Racemic 1 on Cu(110). Racemic (*R*,*R*),(*S*,*S*)-**1** was sublimed onto a clean Cu(110) surface at room temperature and the adlayer was imaged using STM. Images from the as-deposited sample (Figure 2) show distinct dot-like features, measuring about 7 Å across, which is consistent with the size of a single molecule of **1** (the distance between the two stereogenic centers in the crystal structures is approximately

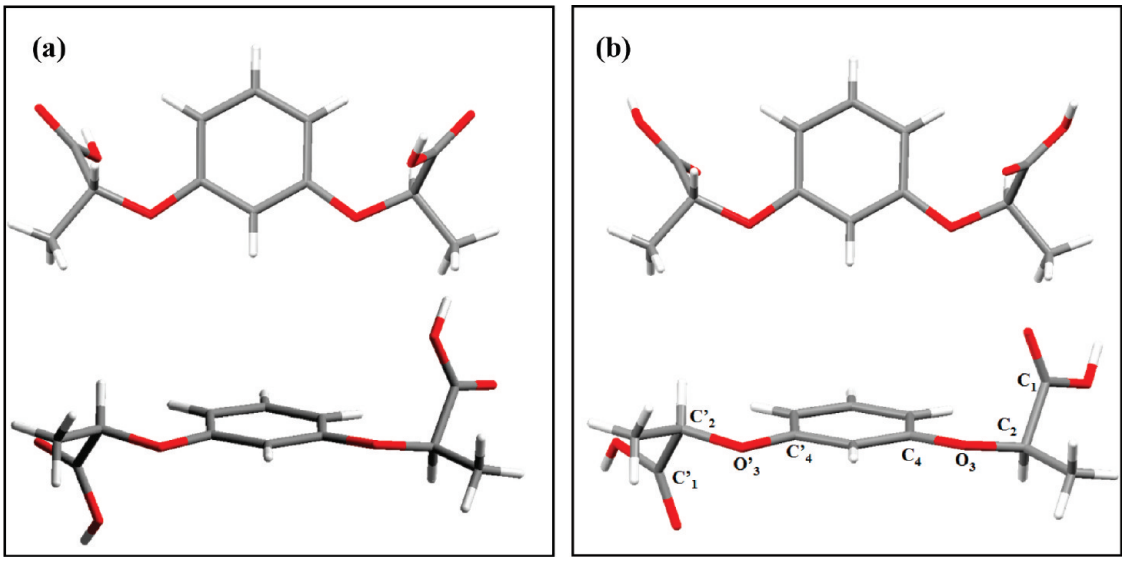

Figure 1. Views of the (*R*,*R*)-**1** conformation in the bulk crystals of the enantiopure compound (a) and in the crystal structure of the racemic compound (*R*,*R*)-**1**/(*S*,*S*)-**1** (b).

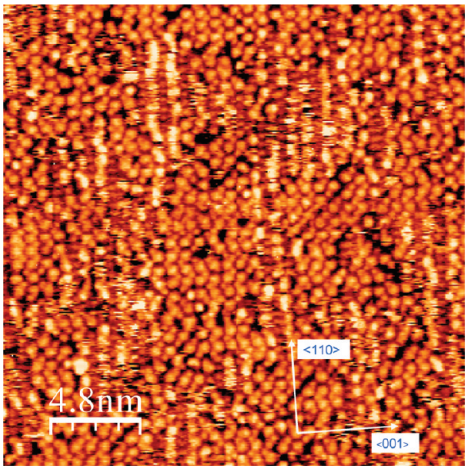

Figure 2. STM image (24 × 24 nm^2, U_{bias} = 0.63 V, I_T = 0.87 nA) of racemic (*R*,*R*),(*S*,*S*)-**1** sublimed onto Cu(110) at room temperature.

7.2 Å), aggregated at the surface but displaying no long-range order. However, amidst this general disorder, occasional small ordered areas are observed, which display short double-molecule chains oriented along specific chiral directions that are approximately ±46° away from the [1$\bar{1}$0] Cu axis (for example, in Figure 2 in the middle there is a row of six pairs of dots). The lengths of these chains generally do not exceed 5 nm in length, but their defined growth direction suggests local aggregation of enantiopure regions; that is, they may represent the very first steps toward the onset of conglomerate formation.

In order to enhance such chiral segregation processes, the sample was annealed to 370 K and the resulting large area STM image (about 2500 nm^2) is shown in Figure 3. This image is striking and shows that the initial general disorder observed at room temperature has now been superseded by a local ordering process in which a multitude of small chiral domains, oriented either +46° or −46° to the [1$\bar{1}$0] direction, are present. However, although the number of chiral domains has increased significantly, their individual size still remains small compared with other monolayer systems of this kind, in this case ranging approximately from 5 to 10 nm in length.

To gain further insight into the nature of these nanoscale chiral domains, high-resolution images were obtained from selected areas (Figure 4). From these pictures. it can be seen that the circular features seen in the large area STM images in fact possess significant submolecular features, displaying five individual elements, of which four give rise to a bulky square part. The fifth feature is found to be attached to either the left-hand or the right-hand edge of the square (rather like a thumbs-up sign), giving rise to two distinct and non-superimposable mirror forms at the surface which we attribute to each enantiomer of **1**. Therefore, a five-spot cartoon can be used to identify the different types of adsorbed molecules, as shown for a disordered area of the surface (Figure 4). We find that four distinct types of images are actually observed, since each enantiomer is found in two positions, rotated by 180° with respect to each other, and as expected from the 2-fold symmetry of the substrate and chirality of the compounds. Thus, we are able to identify both the chirality and orientation of individual molecules at the surface. This situation now provides a powerful means to understand the details of the local chiral organization that are manifest within the STM images (Figure 4).

High resolution images obtained from a local chiral domain formed at the surface (Figure 4, bottom) show that it consists of double-molecule chains. When each molecule is mapped with its five-spot structure, it becomes apparent that the double chain structures are enantiopure and are constructed from antiparallel orientations of the paired molecules. This observation suggests that local chiral segregation toward conglomerate formation has been initiated and local concentrations of enantiopure domains are nucleated. Furthermore, it appears that the enantiopure domains adopt a specific chiral organization. Specific support for this conclusion comes from STM experiments carried with enantiopure (*S*,*S*)-**1** and (*R*,*R*)-**1**, as discussed in the next section.

Enantiopure (*S*,*S*)-1 and (*R*,*R*)-1 on Cu(110). Typical STM images obtained for enantiopure (*S*,*S*)-**1** and (*R*,*R*)-**1** on Cu(110) following deposition at room temperature and

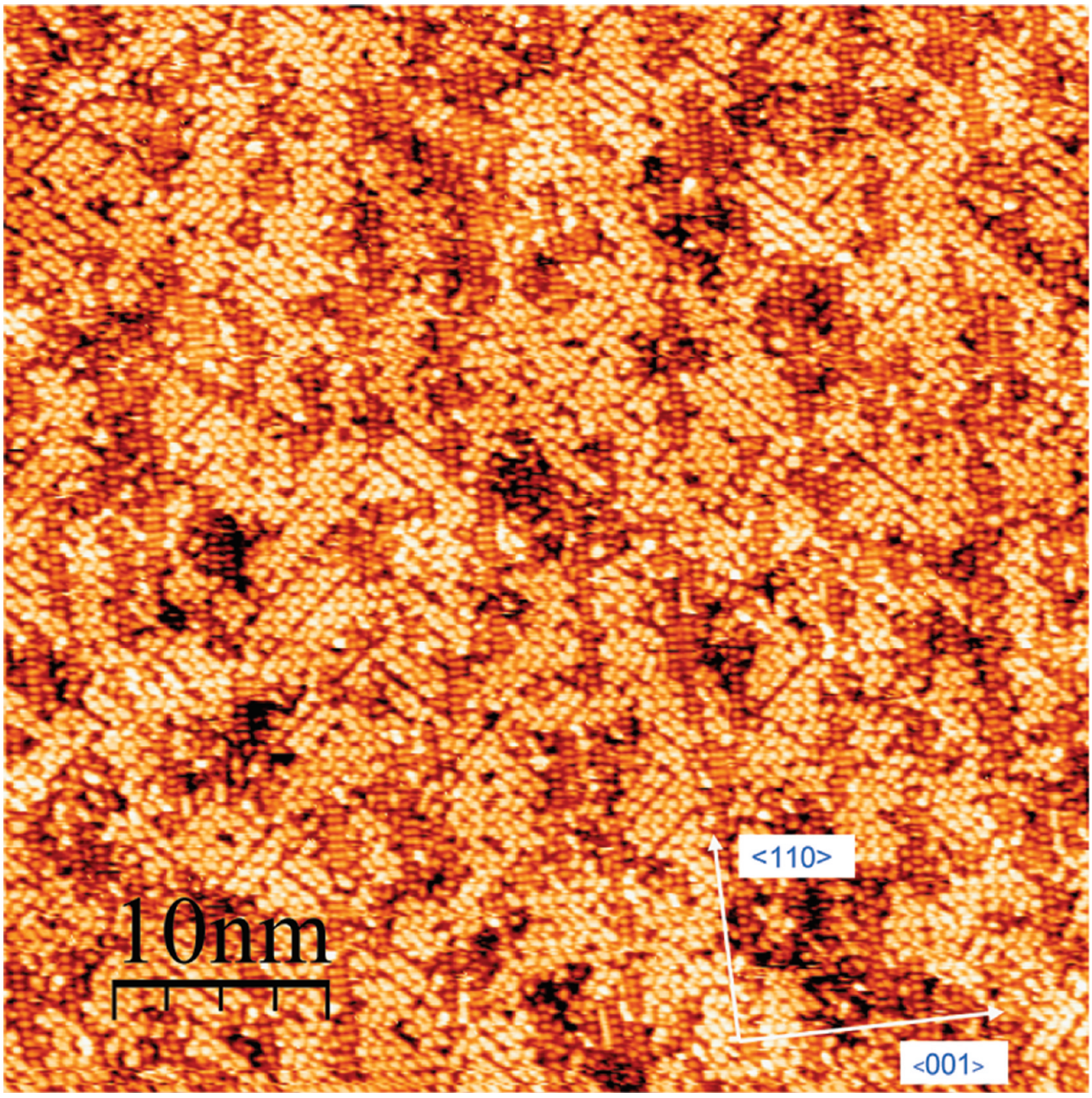

Figure 3. Large-scale STM image (50 × 50 nm^2, U_{bias} = 0.24 V, I_T = 0.65 nA) of racemic (*R*,*R*),(*S*,*S*)-**1** sublimed onto Cu(110) at room temperature and afterward annealed to approximately 370 K.

annealing to between 340 and 370 K are shown in Figure 5. These images show that each enantiopure system assembles into large chiral domains, in which paired-molecule chains grow along nonsymmetry directions aligned at +46° or −46° with respect to the [1$\bar{1}$0] direction of the surface, that is, exactly what is seen in the nanometer scale domains observed for the racemic mixture (Figure 4). It is clear from a comparison of the images in Figure 5 that (*R*,*R*) and (*S*,*S*) form mirror enantiomorphous domains after moderate annealing.

The unit cell dimensions measured from the STM images of (*S*,*S*)-**1** are approximately 1.85 ± 0.1 nm for ***a***′, and 1.05 ± 0.05 nm for ***b***′. The large scale organization is further echoed in the low energy electron diffraction (LEED) data obtained for (*S*,*S*)-**1** (Figure 6), which show clear diffraction spots possessing the superstructure unit cell described by the tensor

$$\Gamma^r = \begin{pmatrix} 3 & -2 \\ 1 & 5 \end{pmatrix} \text{ defined as } \begin{pmatrix} a' \\ b' \end{pmatrix} = \Gamma \begin{pmatrix} a \\ b \end{pmatrix}$$

with *a*, *b* describing the unit vectors of the underlying substrate lattice and *a*′, *b*′ the unit cell vectors of the molecular superlattice. This unit mesh results in unit cell lengths of *a*′ = 18.13 Å and *b*′ = 10.51 Å, which are in excellent agreement with the measured STM distances for the chiral structures of (*S*,*S*)-**1**.

To get further insight into the nature of the adsorbed molecule, we also carried out infrared spectroscopy in the reflection mode (RAIRS). This allows us to investigate the chemical identity of the monolayer. Figure 7 shows the RAIRS spectra obtained of an (*R*,*R*)-**1** adlayer on Cu(110) at room

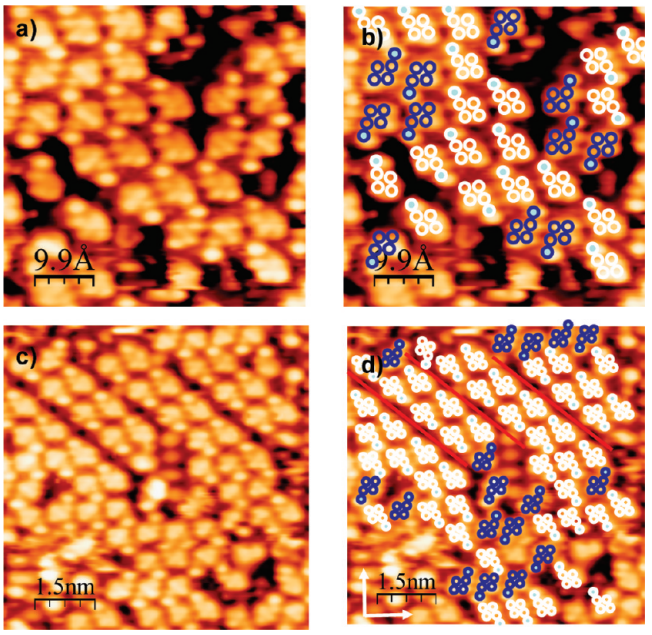

Figure 4. Top: Close-up STM image (50 × 50 Å^2, U_{bias} = 0.29 V, I_T = 0.85 nA) of racemic (*R*,*R*),(*S*,*S*)-**1** deposited on Cu(110) at room temperature and afterward annealed to 370 K. The image depicts an area of molecules of both enantiomers which are identified by different colors, blue and white, respectively, in (b). Bottom: Close-up STM image of enantiomer separation and local domain forming (c, 7.7 × 7.7 nm^2, U_{bias} = 0.28 V, I_T = 0.42 nA). Enantiopure double chains consist of up and down running rows, that is, molecules in one row are rotated by 180° with respect to the molecules in the other row of the double chain. Single molecule identification (d) reveals that extended chain formation is hindered either by the opposite enantiomer or by different, "achiral" molecular conformations. The main directions of the Cu axes are shown in (d) - the vertical one is the ⟨110⟩ and the horizontal the ⟨001⟩ - and apply to all images.

temperature and upon annealing to the temperature at which the chiral organization occurs. Of particular note is that the ν(OH) stretching mode expected at 3513−3518 cm^{-1} for the carboxylic group is not observed and neither is the carbonyl ν(C═O) vibration of the same functionality expected to appear between 1710 and 1790 cm^{-1}. These observations in combination with the presence of a strong symmetric carboxylate stretch, ν_s(COO$^-$) observed at around 1400 cm^{-1} suggest that both carboxylic acid groups of the molecules deprotonate on adsorption. Such deprotonation of carboxylic acid groups to form carboxylate species on Cu(110) is a common behavior that has been observed for a range of species.[14] Apart from these differences, there is good agreement with the rest of the spectrum, suggesting the remaining molecular identity is retained upon adsorption. In addition, it can be seen that annealing to 370 K causes all the bands to sharpen, indicative of an ordering process.[15] This temperature regime corresponds to a change in the LEED pattern to yield an extended chiral organization and the formation of the ordered enantiomorphous chiral phase in STM. Detailed assignments of the RAIRS bands from comparison with calculated gas phase IR spectra for the geometry optimized symmetric molecule are given in the Supporting Information.

Discussion of Enantiomer and Conglomerate Formation on Cu(110) by 1

Combining knowledge of the nature of the adsorbed species and measuring the diameter and profile of molecules from the

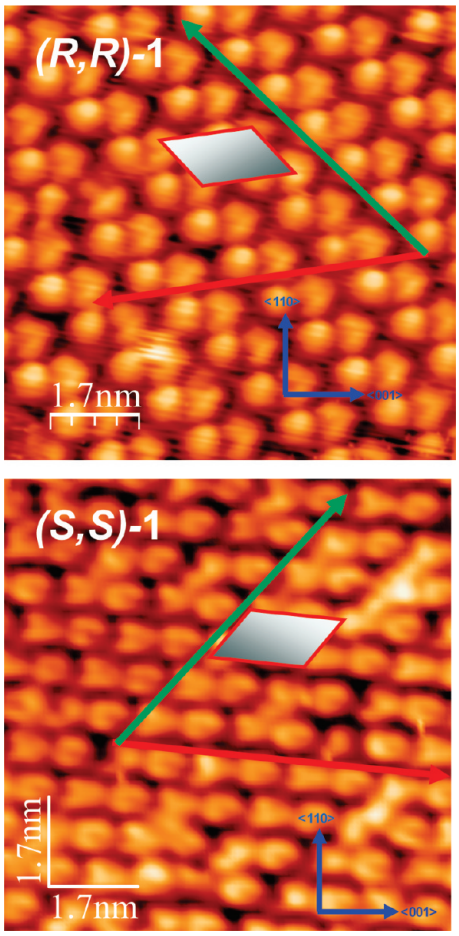

Figure 5. Top: STM image of an (*R*,*R*)-**1** layer annealed to 370 K (10 × 10 nm^2, U_{bias} = −0.88 V, I_T = −0.27 nA). Bottom: the corresponding sample of the (*S*,*S*)-**1** compound.

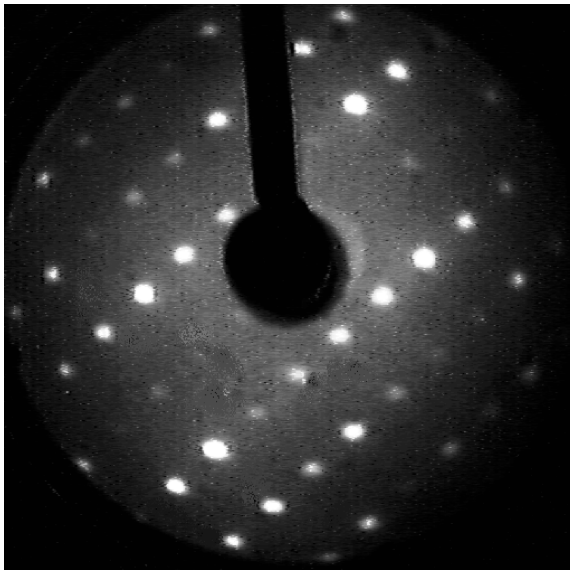

Figure 6. LEED pattern at 35 eV for (*S*,*S*)-**1** monolayer on Cu(110) after annealing to 345 K.

STM data of various domains showing submolecular resolution provide the basis for a local adsorption model of **1** in which each carboxylate group is bonded to the surface at a short-bridge site along the close packed [1$\bar{1}$0] rows of the

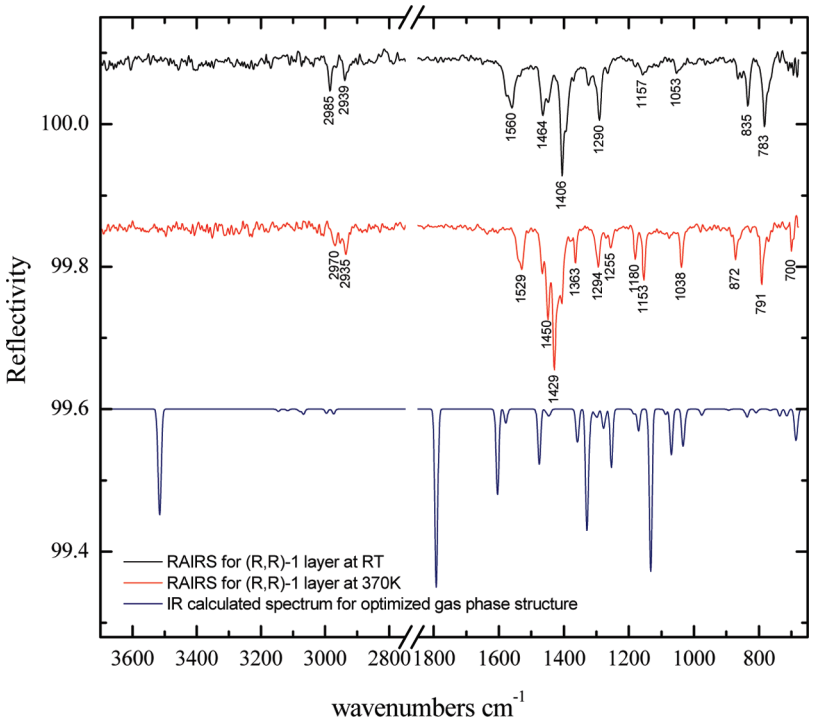

Figure 7. Comparison of experimental RAIRS data at room temperature and 370 K with calculated IR gas phase spectrum for an optimized molecular structure of (*R*,*R*)-**1**.

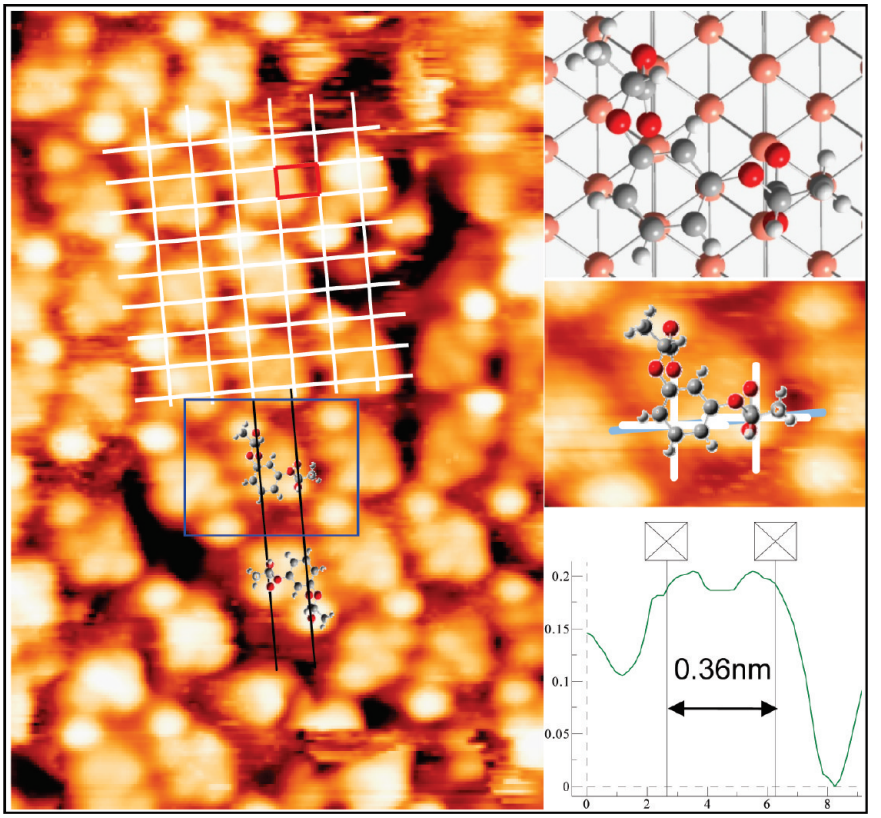

Figure 8. A close-up STM image (U_{bias} = 0.29 V, I_T = 0.85 nA) of racemic (*R*,*R*),(*S*,*S*)-**1** deposited on Cu(110) at room temperature and afterward annealed to 370 K with an overlaid grid showing the unit cell of the surface structure and the proposed adsorption geometry of the molecule. The inset (bottom right) shows a profile of the lozenge part of the molecule along the Cu(001) direction.

metal, an adsorption geometry that is found to occur widely for this functionality at a Cu(110) surface.[16] Taking the molecular asymmetry exhibited in the STM images and the possible molecular configurations into account, we propose the "diagonal" adsorption geometry as indicated by the molecular sketches in Figure 8 to be the most likely one, in which

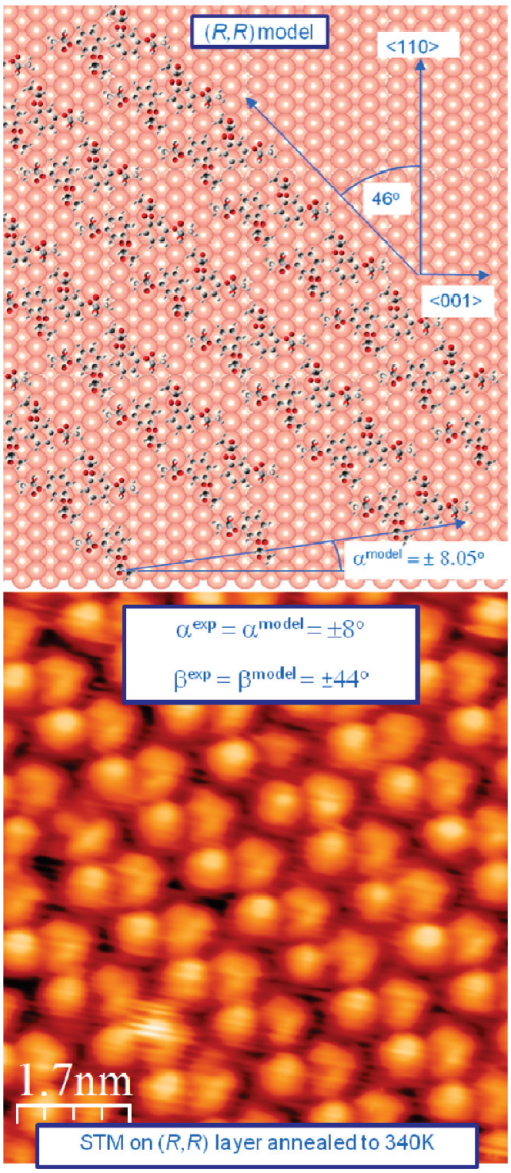

Figure 9. Model of molecular double-chain arrangement of (*R*,*R*)-**1** on Cu(110) after thermal activation of phase change into chiral organization by annealing to 370 K (above). Major directions observed coincide with those of an STM image of (*R*,*R*)-**1** (below).

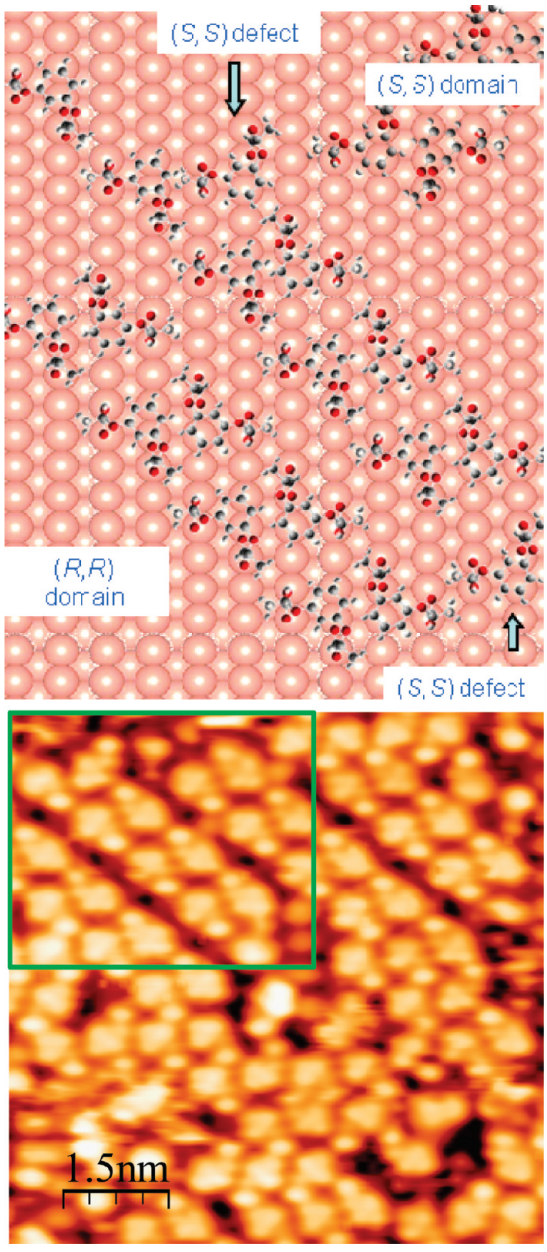

Figure 10. Model of a molecular double-chain arrangement of (*R*,*R*)-**1** in the racemic monolayer showing the interruption of homochiral domains by enantiomers (above), and an area of the STM image (indicated in green) which reveals a similar area (below). See also the cartoon in Figure 4d for a comparison of the defect structure.

the two carboxylate functionalities are adsorbed diagonally across to occupy the short bridge-sites on adjacent [1$\bar{1}$0] rows. This molecular configuration forms the basis for proposing a structural model describing the chiral assemblies.

The STM and LEED data for the enantiopure (*R*,*R*)-**1** and the local adsorption motif constructed above allows one to construct an adsorption model for the enantiomer structure as shown in Figure 9. This model is consistent with the formation of enantiopure double chains aligned at an angle of −46° for (*R*,*R*)-**1** with respect to the ⟨110⟩ direction. Within the double chain, all molecules maintain the same adsorption sites (Figure 9); however, by rotation the molecules prevent Coulomb repulsion that would arise from close contact of the charged carboxylate groups. The same force is proposed to drive the double chain formation by introducing a "spacer" area between neighboring chains to counteract the Coulomb repulsion and to accommodate the compressive stress that is known to accompany carboxylate bonding on the Cu(110) surface.[17] Within the double-molecule rows, the geometry shown in Figure 9 allows the closest possible packing of the molecule with the two benzene rings facing each other. A closer packing would be possible were the carboxyl groups to face each other, but this scenario would be highly unfavorable, again, because of the electrostatic repulsion between the charged carboxylic groups. The juxtaposition of surface bonded carboxylate functionalities at a surface has recently been shown to be a driving factor in determining amino-acid arrangements at surfaces[18] and, it would appear, is also important in this system.

From the structural model, it can be seen that there is strong expression of chirality in the supramolecular organization of the monolayer, where the major growth direction deviates away from the Cu <001> symmetry axis by a large angle of −46°.

There is also, clearly, a direct transmission of chiral information from the nanoscale molecule with its two chiral centers, to the macroscale organization with the mirror (*S*,*S*)-**1** enantiomer, adopting the mirror organization forming double chains aligned at an angle of +46° with respect to the ⟨110⟩ direction (the mirror image to the structure in Figure 9).

Turning now to the racemic mixture, where we were able to distinguish the different enantiomers by submolecular STM imaging, we can unambiguously observe the onset of conglomerate formation upon annealing. However, clearly the process has been arrested and, within the temperature range in which the molecule remains intact, it was impossible to drive macroscopic conglomerate formation. Nevertheless, the preference for conglomerate nucleation is clearly evident, and across the surface one can see the nucleation of enantiopure areas. Remarkably, even at this very earliest onset of aggregation, the organized nuclei, containing literally only tens of molecules, adopt a morphology that is remarkably similar to that of large 2-D crystals of the enantiopure monolayer.

Thus, homochiral molecular chains are observed, adopting a growth direction of 44° with respect to the Cu < 001 > axis. In many cases, the nuclei are an almost identical mimic of the enantiopure phase, and take up the double molecule chain arrangement observed in the enantiopure chiral phase. Our observations suggest that even at the earliest inception of nucleation, way before any recognizable crystallite emerges, the molecular arrangements take up the shapes and habits that resemble those of the fully formed crystals.

The second striking observation from our large scale and small scale STM data is that the conglomerate we image is essentially "nipped in the bud". Discrete organized homochiral nuclei are seen, possessing a boundary that separates them from their environment. Since crystal growth takes place at the boundaries, any molecular impurity that blocks growth at the interface will act as an inhibitor (see model in Figure 10). From our data, it would seem that the role of the inhibitor is very well performed by the mirror enantiomer and that the major obstacle to large scale conglomerate formation is the mutual inhibition exerted by one enantiomer on the growth of the mirror enantiomorph. Thus, each enantiomer is a highly effective inhibitor for the mirror enantiomorph. This result can be viewed as an extreme example of the "tailor-made" additives pioneered by Lahav and co-workers,[4,11,19] where structurally similar molecules are found to be highly effective suppressors of crystallization. Of perhaps even more general interest is that our data support the hypothesis put forward by Pratt-Brock et al.[5] that cross-enantiomer inhibitions exact a very high penalty in the kinetics of conglomerate nucleation and growth, compared to the racemic crystals, and this may be an important factor in determining that less than 10% of molecular crystals display conglomerate behavior.

Concluding Remarks

There is a dramatic contrast between the racemic bulk crystallization of racemic **1** and its adsorption onto Cu(110). While the former is a racemic compound, the latter shows signs of a conglomerate, but the very small domains are curtailed in their growth by enantiomer molecules. Over the whole racemic monolayer (rather than at the local level), one would say that a quite chaotic behavior is observed; an extremely complex system exists with minute areas of what appear to be conglomerates. This reminds us of a description of the onset of chirality in other contexts, where in samples with great inhomogeneities one enantiomer condenses at one position and the mirror enantiomer at another place,[19] as well as the observation of the formation of homochiral sequences of oligopeptides with lower than expected optical purity in conglomerate-type Langmuir layers which might be explained by oligomerization in disordered areas of the films which have small domains.[20] The occurrence of this kind of complex behavior may explain large final enantiomeric excesses seen in three-dimensional crystallization systems.

The somewhat disordered situation (with very local order) observed for the racemate contrasts dramatically with the well-defined monolayers formed by the enantiopure compounds for the same compound in which large domains are formed. Therefore, it seems that, to quote Pratt-Brock,[5] "The presence of molecules of the "wrong" enantiomer will thus inhibit formation of the nucleus and possibly also of the growth of the crystal." We postulate that in the racemic monolayer the enantiomers act as "tailor-made" impurities for each other. This hypothesis gives weight to the theories laid down previously for chiral resolution and crystallization in the presence of chiral impurities,[21] which in turn support our experimental observations. The rate of diffusion on the surface is also expected to play an important role in this system where the adsorbate interacts strongly with the surface: Indeed, Monte Carlo simulations have shown remarkably similar organizational patterns in a racemic system[22] to those shown in Figure 3. In our case, conglomerate nanodomains are observed, but the formation of racemic lattices possibly as a result of kinetic hindering has also been postulated.[23] In a separate context, the effect of population differences in affecting the rates of crystallization of opposite enantiomers has recently been graphically illustrated by STM[24] and underlines the power of scanning probe techniques to map the earliest stages of nucleation and crystallization. The power of the STM experiments in probing these fundamental nanometer scale nucleation and growth phenomena has also been shown here. We believe that these observations and related ones in other contexts will aid greatly in the understanding of the nucleation and growth of racemic compounds and conglomerates.

Experimental Section

Synthesis and Characterization of (*R*,*R*)-2. Resorcinol (1.30 g, 11.8 mmol), (*S*)-methyl lactate (2.7 mL, 28.3 mmol), and triphenylphosphine (7.42 g, 28.3 mmol) were dissolved in dry THF (50 mL) with stirring under an atmosphere of argon, and the mixture was cooled in an ice bath. To this mixture, a solution of diisopropylazodicarboxylate (DIAD) (28.3 mmol) in dry THF (10 mL) was added dropwise over a period of 30 min at 0 °C, and the mixture was allowed to warm up to room temperature with stirring overnight. After addition of water (20 mL), THF was removed in a vacuum and the residue was portioned between dichloromethane and water, and the aqueous phases were extracted once more with dichloromethane. The combined organic phases were dried over sodium sulfate, filtered, and stripped of solvent. The residue was subjected to column chromatography (SiO_2 EtOAc/hexane 1:4) to give ((*R*,*R*)-**2** as a clear oil (1.62 g, 48%). M.F.: $C_{14}H_{18}O_6$; M.W.: 282.29; $[\alpha]_{546}$ = +65.6 deg·cm^2·g^{-1} (*c* = 0.108 g/3 cm^3), CH_2Cl_2); ^{1}H NMR (250 MHz, $CDCl_3$): 7.11 (t, *J* = 8.2, 1H, ArH), 6.45 (dd, *Ja* = 8.2, *Jb* = 2.2, 2H, ArH), 6.38 (t, *J* = 2.2, 1H, ArH), 4.71 (q, *J* = 6.9, 1H, -OC<u>H</u>CH$_3$CO−), 3.72 (s, 3H, −COO<u>Me</u>), 1.57 (d, *J* = 6.9, -OCH<u>CH$_3$</u>CO−) ppm. FT-IR (*KBr*): 2991 (m, -OCH<u>CH$_3$</u>), 2955 (m, -OCH<u>CH$_3$</u>), 1757 (s, <u>CO</u>OCH$_3$), 1738 (s, <u>CO</u>OCH$_3$), 1673 (w), 1604 (s, phenyl), 1687 (s), 1491 (s), 1454 (s), 1376 (s), 1283 (s), 1209 (s), 1181 (s), 1157 (s), 1135 (s), 1097 (s), 1053 (s), 977 (m), 835 (m), 768 (m), 685 (m) cm^{-1}; Elemental Analysis (%) calculated: C 59.57, H 6.43, found C 59.73, H 6.22.

Synthesis and Characterization of (*R*,*R*)-1. To a solution of (*R*,*R*)-**2** (1.3 g, 4.61 mmol) in methanol (30 mL) 2 N NaOH (6.9 mL) was added and the mixture was stirred at room temperature overnight. The reaction mixture was concentrated, diluted with water (20 mL), and acidified with concentrated HCl to pH 2. After three extractions with EtOAc, the organic phases were dried over sodium sulfate, filtered, and the solvent removed in a vacuum. 1.30 g of (*R*,*R*)-**1** was obtained as a white solid (94% yield).

M.F.: $C_{12}H_{14}O_6$; M.W.: 254.08; M.P.:130 °C (lit. 132−140 °C)[25] $[\alpha]_{546} = +38.4\ deg \cdot cm^2 \cdot g^{-1}$ (c = 0.096 g/3 cm^3, CH_2Cl_2); ^{1}H NMR (250 MHz, DMSO-d_6): 8.30 (s, OH), 7.14 (t, J = 8.2, 1H, ArH), 6.42 (dd, Ja = 8.2, Jb = 2.2, 2H, ArH), 6.33 (t, J = 2.2, 1H, ArH), 4.75 (q, J = 6.9, 1H, -OCHCH$_3$CO−), 1.46 (d, J = 6.7, -OCHCH$_3$CO−) ppm; UV−vis ($CHCl_3$) λ_{max}/nm (ε/ mol L^{-1} cm^{-1}): 206 (788), 273 (220); FT-IR (KBr): 3117 (s, OH), 2992 (m, -OCHCH$_3$), 2942 (m, -OCHCH$_3$), 1715 (s, COOH), 1670 (m, COOH), 1612 (s, phenyl), 1586 (m, phenyl), 1495 (s), 1481 (s), 1453 (m), 1408 (s), 1372 (w), 1332 (m), 1289 (s), 1232 (s), 1169 (s), 1151 (s), 1087 (s), 1042 (s), 988 (m), 884 (m), 857 (m), 752 (m), 683 (m) cm^{-1}; Elemental Analysis (%) calculated C 56.69, H 5.55, found C 56.91, H 5.67.

Synthesis and Characterization of (*S*,*S*)-2. (*S*,*S*)-**2** was obtained as a clear oil following the same synthetic procedure used for (*R*,*R*)-**2** (48% yield). M.F.: $C_{14}H_{18}O_6$; M.W.: 282.11; $[\alpha]_{546}$= −73.3 $deg \cdot cm^2 \cdot g^{-1}$ (c = 0.129 g/3 cm^3, CH_2Cl_2); ^{1}H NMR (250 MHz, $CDCl_3$): 7.11 (t, J = 8.2, 1H, ArH), 6.45 (dd, Ja = 8.2, Jb = 2.2, 2H, ArH), 6.38 (t, J = 2.2, 1H, ArH), 4.71 (q, J = 6.9, 2H, -OCHCH$_3$CO−), 3.72 (s, 6H, −COOMe), 1.57 (d, J = 6.9, 6H, -OCHCH$_3$CO−) ppm; UV−vis ($CHCl_3$) λ_{max}/nm (ε/mol L^{-1} cm^{-1}): 215 (762), 273 (185); FT-IR (KBr): 2991 (m, -OCHCH$_3$), 2955 (m, -OCHCH$_3$), 1757 (s, COOCH$_3$), 1738 (s, COOCH$_3$), 1673 (w), 1604 (s, phenyl), 1687 (s), 1491 (s), 1454 (s), 1376 (s), 1283 (s), 1209 (s), 1181 (s), 1157 (s), 1135 (s), 1097 (s), 1053 (s), 977 (m), 835 (m), 768 (m), 685 (m) cm^{-1}; elemental analysis (%) calculated: C 59.57, H 6.43, found C 59.78, H 6.18.

Synthesis and Characterization of (*S*,*S*)-1. (*S*,*S*)-**1** was obtained as white solid following the same synthetic procedure used for (*R*,*R*)-**1** (94% yield). M.F.: $C_{12}H_{14}O_6$; M.W.: 254.08; M.P.: 130 °C; $[\alpha]_{546}$ = $-36.6\ deg \cdot cm^2 \cdot g^{-1}$ (c = 0.091 M, CH_2Cl_2); ^{1}H NMR (250 MHz, DMSO-d_6): 8.30 (s, 2H, OH), 7.14 (t, J = 8.2, 1H, ArH), 6.42 (dd, Ja = 8.2, Jb = 2.2, 2H, ArH), 6.33 (t, J = 2.2, 1H, ArH), 4.75 (q, J = 6.9, 2H, -OCHCH$_3$CO−), 1.46 (d, J = 6.7, 6H, -OCHCH$_3$CO−) ppm; UV−vis ($CHCl_3$) λ_{max}/nm (ε/mol L^{-1} cm^{-1}): 206 (778), 273 (235); FT-IR (KBr): 3117 (s, OH), 2992 (m, -OCHCH$_3$), 2942 (m, -OCHCH$_3$), 1715 (s, COOH), 1670 (m, COOH), 1612 (s, phenyl), 1586 (m, phenyl), 1495 (s), 1481 (s), 1453 (m), 1408 (s), 1372 (w), 1332 (m), 1289 (s), 1232 (s), 1169 (s), 1151 (s), 1087 (s), 1042 (s), 988 (m), 884 (m), 857 (m), 752 (m), 683 (m) cm^{-1}; Elemental Analysis (%) calculated C 56.69, H 5.55, found C 56.94, H 5.67.

IR Spectra of the Racemic Mixture (*R*,*R*)-1/(*S*,*S*)-1 in Their Crystal Structure. FT-IR (HATR): 2998 (s, OH), 2943 (m, -OCHCH$_3$), 2644 (w), 2556 (w), 2465 (w), 1712 (s, COOH), 1599 (s, phenyl), 1583 (s, phenyl), 1493 (m), 1477 (m), 1453 (m), 1422(m), 1370 (w), 1326 (m), 1282 (s), 1233 (s), 1181 (s), 1157 s, 1135 (s), 1090 (s), 1046 (s), 993 (m), 918 (s), 853 (s), 762 (s), 686 (s) cm^{-1}.

Calculation Details for IR Spectra of the Enantiopure (*R*,*R*)-1 in Gas Phase. DFT calculations of (*R*,*R*)-**1** in the gas phase were performed in a 20 × 15 × 15 $Å^3$ supercell. Structures were relaxed until forces were less than 0.005 eV/atom. The plane wave basis has been expanded up to a cutoff energy of 400 eV. It was found that the symmetric structure with two internal hydrogen-bonds is by 60 meV more stable than the asymmetric structure with only one internal hydrogen-bond between the carbonyl and the ether group.

Details of Monolayer Studies of 1 on Cu(110). The clean Cu(110) surface was prepared by argon ion sputtering at 500 eV followed by annealing to 800 K. Low energy electron diffraction (LEED) was utilized to check the cleanliness of the sample, with a sharp (1 × 1) pattern characteristic of clean Cu(110). Enantiopure and racemic **1** were dosed from an electrically heated glass tube, separated from the main chamber by a gate valve and differentially pumped by a turbomolecular pump. Each sample of **1** was thoroughly outgassed to ensure sample purity prior to dosing. In all experiments, the Cu(110) crystal was held at room temperature during dosing.

STM images were recorded, at room temperature, in an ultra high vacuum (UHV) chamber, with a base pressure of 2×10^{-10} mbar, and fitted with a Specs Aarhus 150 STM operated in constant current mode with an electrochemically etched tungsten tip. The bias voltage was applied to the sample.

RAIRS and LEED experiments were performed in a multi-technique UHV chamber interfaced to a Mattson 6020 FTIR spectrometer via ancillary optics and KBr windows. A nitrogen cooled HgCdTe detector allowed the IR spectral range of 650−4000 cm^{-1} to be accessed. The resolution of the spectrometer was set to 4 cm^{-1} and 250 scans were coadded. The spectrum of the clean sample was taken as a background reference, R^0, at the beginning of the experiments. Spectra of the adsorbed layer are displayed as the ratio $(R - R^0)/R^0$ with respect to the clean sample spectrum.

Acknowledgment. The research leading to these results has received funding from the European Community's Seventh Framework Programme under Grant Agreement No. NMP4-SL-2008-214340, project RESOLVE, and the Marie Curie Research Training Network CHEXTAN (MRTN-CT-2004-512161), the EU Marie Curie Host Fellowship Program TANSAS (MTKD-CT-2005-029689). We are also grateful to the Generalitat de Catalunya (2009 SGR 158) for research support for D.B.A., and the UK EPSRC for support for R.R.. We also thank the referees for constructive criticisms which helped improve the manuscript.

Supporting Information Available: Crystallographic information files; tables of crystallographic data for (*R*,*R*)-**1** and racemate (*R*,*R*)-**1**/(*S*,*S*)-**1**; figures of (*R*,*R*)-**1** and (*R*,*R*)-**1**/(*S*,*S*)-**1** crystal structures; (*R*,*R*)-**1** in the optimized gas phase structure; table of assignments for IR active modes. This material is available free of charge via the Internet at http://pubs.acs.org.

References

(1) (a) Collins, A. N.; Sheldrake, G. N.; Crosby, J., Eds. *Chirality in Industry Vols I and II*; J. Wiley & Sons: Chichester, 1992 and 1997. (b) Nugent, W. A.; Rajanbabu, T. V.; Burk, M. J. *Science* **1993**, *259*, 479–483. (c) Ding, J.; Armstrong, D. W. *Chirality* **2005**, *17*, 281–292. (d) Amabilino, D. B.; Veciana, J. *Top. Curr. Chem.* **2006**, *265*, 253–302. (e) Sancho, R.; Minguillon, C. *Chem. Soc. Rev.* **2009**, *38*, 797–805.

(2) (a) Jacques, J.; Collet, A.; Wilen, S. H. *Enantiomers, Racemates and Resolutions*; Krieger Publishing Co.: Malabar, FL, 1994. (b) Pérez-García, L.; Amabilino, D. B. *Chem. Soc. Rev.* **2002**, *31*, 342–356. (c) Pérez-García, L.; Amabilino, D. B. *Chem. Soc. Rev.* **2007**, *36*, 941–967.

(3) (a) Collet, A.; Brienne, M.-J.; Jacques, J. *Chem. Rev.* **1980**, *80*, 215–230. (b) Coquerel, G.; Amabilino, D. B. In *Chirality at the Nanoscale*; Amabilino, D. B., Eds.; Wiley-VCH: New York, 2009.

(4) Addadi, L.; Berkovitch-Yellin, Z.; Weissbuch, I.; Lahav, M.; Leiserowitz, L. *Top. Stereochem.* **1986**, *16*, 1–85.

(5) Pratt-Brock, C.; Schweizer, W. B.; Dunitz, J. D. *J. Am. Chem. Soc.* **1991**, *113*, 9811–9820.

(6) (a) Davey, R. J.; Allen, K.; Blagden, N.; Cross, W. I.; Lieberman, H. F.; Quayle, M. J.; Righini, S.; Seton, L.; Tiddy, G. J. T. *CrystEngComm* **2002**, 257–264. (b) Erdemir, D.; Lee, A. Y.; Myerson, A. S. *Acc. Chem. Res.* **2009**, *42*, 621–629. (c) Kellogg, R. M.; Kaptein, B.; Vries, T. R. *Top. Curr. Chem.* **2007**, *269*, 159–198.

(7) (a) Raval, R. *Chem. Soc. Rev.* **2009**, *38*, 707–721. (b) Haq, S.; Liu, N.; Humblot., V.; Jansen, A. P. J.; Raval, R. *Nat. Chem.* **2009**, *1*, 409–414.

(8) (a) Lopinski, G. P.; Moffatt, D. J.; Wayner, D. D. M.; Wolkow, R. A. *Nature* **1998**, *392*, 909–911. (b) Bohringer, M.; Morgenstern, K.; Schneider, W.-D.; Berndt, R. *Angew. Chem., Int. Ed.* **1999**, *38*, 821–823.

(9) Elemans, J. A. A. W.; De Cat, I.; Xu, H.; De Feyter, S. *Chem. Soc. Rev.* **2009**, *38*, 722–736.

(10) (a) Barlow, S. M.; Raval, R. *Surf. Sci. Rep.* **2003**, *50*, 201. (b) Humblot, V.; Barlow, S. M.; Raval, R. *Prog. Surf. Sci.* **2004**, *76*, 1–19. (c) Ernst, K. H. *Top. Curr. Chem.* **2006**, *265*, 209–252. (d) Ortega Lorenzo, M.; Baddeley, C. J.; Muryn, C.; Raval, R. *Nature* **2000**, *404*, 376–379. (e) Humblot, V.; Ortega Lorenzo, M.; Baddeley, C. J.; Haq, S.; Raval, R. *J. Am. Chem. Soc.* **2004**, *126*, 6460–6469.

(11) (a) Weissbuch, I.; Kuzmenko, I.; Berfeld, M.; Leiserowitz, L.; Lahav, M. *J. Phys. Org. Chem.* **2000**, *13*, 426–434. (b) Weissbuch, I.; Leiserowitz, L.; Lahav, M. *Top. Curr. Chem.* **2005**, *259*, 123–165.
(12) (a) Mitsunobu, O. *Synthesis* **1981**, 1–28. (b) Swamy, K. C. K.; Kumar, N. N. B.; Balaraman, E.; Kumar, K. V. P. *Chem. Rev.* **2009**, *109*, 2551–2651.
(13) Linares, M.; Iavicoli, P.; Psychogyiopoulou, K.; Beljonne, D.; De Feyter, S.; Amabilino, D. B.; Lazzaroni, R. *Langmuir* **2008**, *24*, 9566–9574.
(14) (a) Hayden, B. E.; Prince, K.; Woodruff, D. P.; Bradshaw, A. M. *Surf. Sci.* **1983**, *133*, 589–604. (b) Woodruff, D. P.; McConville, C. F.; Kilcoyne, A. L. D.; Lindner, T.; Somers, J.; Surman, M.; Paolucci, G.; Bradshaw, A. M. *Surf. Sci.* **1988**, *201*, 228–244. (c) Bowker, M.; Haq, S.; Holroyd, R.; Parlett, P. M.; Poulston, S.; Richardson, N. *J. Chem. Soc.-Faraday Trans.* **1996**, *92*, 4683–4686. (d) Frederick, B. G.; Leibsle, F. M.; Haq, S.; Richardson, N. V. *Surf. Rev. Lett.* **1996**, *3*, 1523–1546. (e) Ortega Lorenzo, M.; Haq, S.; Bertrams, T.; Murray, P.; Raval, R.; Baddeley, C. J. *J. Phys. Chem. B* **1999**, *103*, 10661–10669. (f) Ortega Lorenzo, M.; Baddeley, C. J.; Muryn, C.; Raval, R. *Nature* **2000**, *404*, 376–379. (g) Barlow, S. M.; Raval, R. *Surf. Sci. Rep.* **2003**, *50*, 201–341. (h) Humblot, V.; Ortega Lorenzo, M.; Baddeley, C. J.; Haq, S.; Raval, R. *J. Am. Chem. Soc.* **2004**, *126*, 6460–6469. (i) Haq, S.; Massey, A.; Moslemzadeh, N.; Robin, A.; Barlow, S. M.; Raval, R. *Langmuir* **2007**, *23*, 10694–10700.
(15) Raval, R.; Parker, S. F.; Chesters, M. A. *J. Chem. Soc. Faraday Transact.* **1996**, *92*, 2611–2614.
(16) (a) Rankin, R. B.; Sholl, D. S. *Surf. Sci.* **2004**, *548*, 301–308. (b) James, J. N.; Sholl, D. S. *Curr. Opin. Colloid Interface Sci.* **2008**, *13*, 60–64. (c) Jones, G.; Jones, L. B.; Thibault-Starzyk, F.; Seddon, E. A.; Raval, R.; Jenkins, S. J.; Held, G. *Surf. Sci.* **2006**, *600*, 1924–1935. (d) Sayago, D. I.; Polcik, M.; Nisbet, G.; Lamont, C. L. A.; Woodruff, D. P. *Surf. Sci.* **2005**, *590*, 76–87. (e) Forster, M.; Dyer, M.; Persson, M.; Raval, R. *J. Am. Chem. Soc.* **2009**, *131*, 10173–10181.
(17) Hermse, C. G. M.; Van Bavel, A. P.; Jansen, A. P. J.; Barbosa, L. A. M. M.; Sautet, P.; Van Santen, R. A. *J. Phys. Chem. B* **2004**, *108*, 11035–11043.
(18) Forster, M.; Dyer, M. S.; Persson, M.; Raval, R. *Angew. Chem., Int. Ed. Engl.* **2010**, *49*, 2344–2348.
(19) Plasson, R.; Kondepudi, D. K.; Asakura, K. *J. Phys. Chem. B* **2006**, *110*, 8481–8487.
(20) Weissbuch, I.; Bolbach, G.; Zepik, H.; Shavit, E.; Tang, M.; Frey, J.; Jensen, T. R.; Kjaer, K.; Leiserowitz, L.; Lahav, M. *J. Am. Chem.. Soc.* **2002**, *124*, 9093–9104.
(21) (a) Weissbuch, I.; Lahav, M.; Leiserowitz, L. *Cryst. Growth Des.* **2003**, *3*, 125–150. (b) Kondepudi, D. K.; Crook, K. E. *Cryst. Growth Des.* **2005**, *5*, 2173–2179.
(22) Unac, R. O.; Vidales, A. M.; Zgrablich, G. *Ads. Sci. Technol.* **2009**, *27*, 633–641.
(23) Parschau, M.; Fasel, R.; Ernst, K.-H. *Cryst. Growth Des.* **2008**, *8*, 1890–1896.
(24) Haq, S.; Liu, N.; Humblot, V.; Jansen, A. P. J.; Raval, R. *Nat. Chem.* **2009**, *1*, 409–414.
(25) Burkard, U.; Effenberger, F. *Chem. Ber.* **1986**, *119*, 1594–1612.